diabetes
American Diabetes Association

Macrophage SHP2 Deficiency Alleviates Diabetic Nephropathy via Suppression of MAPK/NF-κB–Dependent Inflammation

Xue Han, Jiajia Wei, Ruyi Zheng, Yu Tu, Mengyang Wang, Lingfeng Chen, Zheng Xu, Lei Zheng, Chao Zheng, Qiaojuan Shi, Huazhong Ying, and Guang Liang

Diabetes 2024;73(5):780–796 | https://doi.org/10.2337/db23-0700

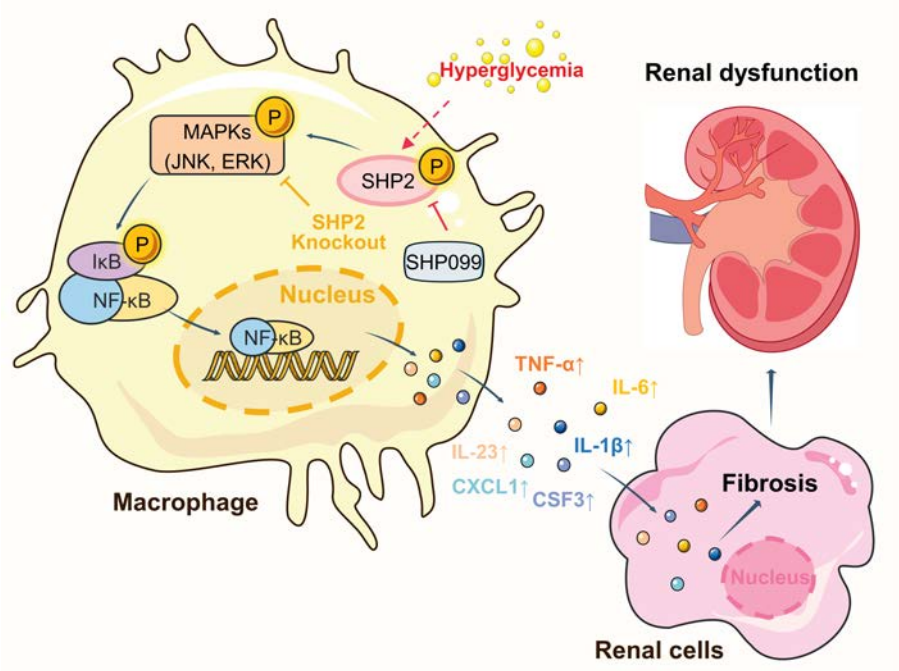

The macrophage-specific SHP2 knockout in mouse models ameliorated diabetes-induced renal dysfunction and fibrosis. SHP2 deletion suppressed the activation of mitogen-activated protein kinase (MAPK) and nuclear factor-κB (NF-κB) signaling pathways, thereby inhibiting the expression of inflammatory cytokines and chemokines. These macrophage-derived cytokines promoted phenotype transition and fibrotic responses in renal cells. IL, interleukin; TNF, tumor necrosis factor.

Macrophage SHP2 Deficiency Alleviates Diabetic Nephropathy via Suppression of MAPK/NF-κB–Dependent Inflammation

Xue Han,[1–3] Jiajia Wei,[1] Ruyi Zheng,[1] Yu Tu,[1] Mengyang Wang,[4] Lingfeng Chen,[2] Zheng Xu,[2] Lei Zheng,[2] Chao Zheng,[5] Qiaojuan Shi,[1] Huazhong Ying,[1] and Guang Liang[2,3]

Diabetes 2024;73:780–796 | https://doi.org/10.2337/db23-0700

Increasing evidence implicates chronic inflammation as the main pathological cause of diabetic nephropathy (DN). Exploration of key targets in the inflammatory pathway may provide new treatment options for DN. We aimed to investigate the role of Src homology 2–containing protein tyrosine phosphatase 2 (SHP2) in macrophages and its association with DN. The upregulated phosphorylation of SHP2 was detected in macrophages in both patients with diabetes and in a mouse model. Using macrophage-specific SHP2-knockout (SHP2-MKO) mice and $SHP2^{fl/fl}$ mice injected with streptozotocin (STZ), we showed that SHP2-MKO significantly attenuated renal dysfunction, collagen deposition, fibrosis, and inflammatory response in mice with STZ-induced diabetes. RNA-sequencing analysis using primary mouse peritoneal macrophages (MPMs) showed that SHP2 deletion mainly affected mitogen-activated protein kinase (MAPK) and nuclear factor-κB (NF-κB) signaling pathways as well as MAPK/NF-κB–dependent inflammatory cytokine release in MPMs. Further study indicated that SHP2-deficient macrophages failed to release cytokines that induce phenotypic transition and fibrosis in renal cells. Administration with a pharmacological SHP2 inhibitor, SHP099, remarkably protected kidneys in both type 1 and type 2 diabetic mice. In conclusion, these results identify macrophage SHP2 as a new accelerator of DN and suggest that SHP2 inhibition may be a therapeutic option for patients with DN.

ARTICLE HIGHLIGHTS

- Phosphorylated Src homology 2–containing protein tyrosine phosphatase 2 (SHP2) levels in macrophages are increased in both patients and mice with diabetic neuropathy (DN).
- Macrophage SHP2 knockout prevents renal inflammation and DN in diabetic mice.
- SHP2 deletion suppresses the activation of mitogen-activated protein kinase and nuclear factor-κB signaling pathways, thereby inhibiting inflammation in macrophages.
- Pharmacological inhibition of SHP2 protects against DN in both type 1 and type 2 diabetic mice.

Diabetic nephropathy (DN) represents a major cause of end-stage renal disease (1). It occurs in patients with type 1 (T1D) or type 2 diabetes (T2D). Its impacts are manifested as intraglomerular hypertension, glomerular hyperfiltration, and extracellular matrix expansion, finally resulting in proteinuria and progressive renal dysfunction (2,3). Nevertheless, antidiabetic therapeutic approaches only delay the progression of DN; effective remedies for DN management are rare. Accordingly, exploring the pathophysiological mechanisms for promptly managing this disorder is paramount.

[1]Zhejiang Provincial Key Laboratory of Laboratory Animals and Safety Research, Hangzhou Medical College, Hangzhou, China
[2]Zhejiang Traditional Chinese Medicine Key Laboratory of Pharmacology and Translational Research of Natural Products, School of Pharmaceutical Sciences, Hangzhou Medical College, Hangzhou, China
[3]Chemical Biology Research Center, School of Pharmaceutical Sciences, Wenzhou Medical University, Wenzhou, China
[4]Department of Pharmacology, College of Pharmacy, Beihua University, Jilin, China
[5]Department of Endocrinology, Second Affiliated Hospital, School of Medicine, Zhejiang University, Hangzhou, China

Corresponding author: Guang Liang, wzmcliangguang@163.com, Huazhong Ying, yhz0101@126.com, or Qiaojuan Shi, shiqiaojuan@163.com

Received 30 August 2023 and accepted 13 February 2024

This article contains supplementary material online at https://doi.org/10.2337/figshare.25259746.

X.H. and J.W. contributed equally to this work.

It is widely known that chronic inflammation plays a crucial role in the development of DN (4,5). In diabetes, various molecules involved in the inflammatory response, including proinflammatory cytokines, chemokines, and adhesion molecules, can perpetuate renal damage, leading to glomerulosclerosis and interstitial fibrosis. These cytokines, in turn, contribute to the recruitment and activation of immune cells, mainly with the inclusion of macrophages and neutrophils, via a positive feedback loop (6,7). Macrophage recruitment further results in the production of inflammatory cytokines that decrease the degradation of matrix proteins and promote glomerulosclerosis and renal fibrosis in DN (8–10). These studies reveal a rather important role of macrophage-mediated inflammation in DN. However, the precise mechanism and the related targets by which diabetes induces the inflammatory response in macrophages remain a puzzle.

Src homology 2–containing protein tyrosine phosphatase 2 (SHP2) belongs to the nonreceptor protein tyrosine phosphatase family (11). Abnormal activation of SHP2 has been implicated in the various pathogeneses of disorders including cancer, inflammation-related diseases, and metabolic syndrome via the activation the diverse downstream signal transduction pathways of JAK2/STAT3, Ras/mitogen-activated protein kinase (MAPK), and transforming growth factor-β (TGF-β)/Smad3 (12–14). Although no agents have been approved for the SHP2 target, several SHP2 inhibitors are in clinical trials for cancer, especially TNO-155, which is now in phase 2 (15). We and other groups have found that SHP2 is also associated with the regulation of inflammatory disorders (16,17). We previously reported that SHP2 was highly expressed in macrophages in a lipopolysaccharide-induced acute lung injury mouse model, and inhibition of SHP2 increased animal survival via downregulation of MAPK-mediated inflammation (16). Zhu et al. (17) reported that SHP2 deficiency in macrophages weakened nuclear factor-κB (NF-κB) activation and proinflammatory cytokine gene expression, subsequently resulting in the improvement of psoriasis-like skin inflammation. Given the regulatory function of SHP2 in immune responses, we hypothesized that excessive inflammation was an underlying mechanism of SHP2 implicated in DN.

In this study, we elucidated the pivotal role of SHP2 in the pathogenesis of DN. We found that macrophage SHP2 was significantly activated in diabetic mouse kidneys, indicating its significance in the progression of DN. We demonstrated that SHP2 activated the MAPK/NF-κB proinflammatory signaling pathway in macrophages. Macrophage SHP2 deficiency and pharmacological SHP2 inhibition each alleviated DN via suppression of MAPK/NF-κB–dependent inflammation. This finding potentially unveils SHP2 as a prospective therapeutic target in combating DN.

RESEARCH DESIGN AND METHODS

Experimental Animals

All animal studies were performed strictly according to the National Institutes of Health Guidelines for the Care and Use of Laboratory Animals. They were euthanized after approval by the Ethics Committee of Laboratory Animal Care and Welfare, Hangzhou Medical College (approval no. ZJCLA-IACUC-20040082; Hangzhou, China). Eight-week-old male *db/db* (C57BLKS/J-*lepr*^{db}/*lepr*^{db}) mice and their nondiabetic *db/m* littermates and 8-week-old male C57BL/6J mice were purchased from the Laboratory Animal Center of Hangzhou Medical College. Nonobese diabetic (NOD)/ShiLtJ mice and nondiabetic NOR/LtJ mice were obtained at age 23 weeks from the Laboratory Animal Center of Hangzhou Medical College. Only female NOD mice were used in this study because of the higher incidence of diabetes than in male mice. Macrophage-specific SHP2-knockout (SHP2-MKO) mice were generated by crossing SHP2-floxed mice with Lyz2-Cre transgenic mice obtained from Professor Yang Sun (Nanjing University, Nanjing, China). All mice were accommodated for 1 week before the animal experiments. The mice used in this study were maintained under standardized conditions. They were housed in a controlled environment with an ambient temperature of 22°C and relative humidity of 40–60%. A 12-h light-dark cycle was implemented to simulate natural day-night patterns. Throughout the experimental period, the mice had ad libitum access to food and water. Stringent measures were taken to ensure animal welfare, including efforts to minimize the number of animals used and alleviate any potential suffering experienced by the subjects.

Animal Studies

All animals participating in the current inquiry were acclimatized to the laboratory conditions before use. For the T1D mouse model, C57BL/6J mice were intraperitoneally injected with streptozotocin (STZ; Sigma-Aldrich, St Louis, MO) at a single dose of 100 mg/kg formulated in 100 mmol/L citrate buffer (pH 4.5). The control animals received only an equivalent citrate buffer. One week later, a fasting blood glucose (FBG) measurement was taken, and mice with FBG ≥12 mmol/L were labeled as diabetic. Mice with STZ-induced diabetes were randomly divided into three experimental groups (n = 7 per group): vehicle group (0.5% CMC-Na solution), low-dose SHP099 group (2.5 mg/kg; purity ≥99.80%; MedChemExpress, Bloomfield, NJ), and high-dose SHP099 group (5 mg/kg). SHP099, an experimental compound targeting SHP2, was administered daily via oral gavage to the experimental group for 8 weeks. Conversely, the control group received an equivalent volume of a vehicle solution over the same timeframe. SHP2$^{fl/fl}$ and SHP2-MKO mice were induced to develop T1D with STZ, as described above. Age-matched SHP2$^{fl/fl}$ and SHP2-MKO mice served as control groups.

For the T2D mouse model, *db/db* mice comprised the SHP099 (5 mg/kg) and vehicle groups, receiving treatment for 8 weeks by gavage every other day. Age-matched *db/m* mice were treated with a vehicle according to the same schedule as that of the nondiabetic control group.

NOD mice were confirmed to have diabetes after 2 consecutive days of FBG >12 mmol/L. Diabetic NOD mice

received SHP099 (at 5 mg/kg via gavage; NOD+SHP099 group) or vehicle (NOD group) for 6 weeks every other day. In one group (NOD+SHP099+withdrawal), mice were treated with SHP099 for 6 weeks (5 mg/kg) and then treated with normal saline for an extra 2 weeks. Age-matched NOR mice were treated with vehicle as the control group (NOR group).

Blood glucose and body weight were measured weekly for all the above-described animal groups. At the end of each experiment, the mice were anesthetized with an intraperitoneal injection of phenobarbital sodium at 40 mg/kg body weight. After that, blood samples and kidney tissues were harvested and processed for additional studies. Urine from the mice was collected using metabolic cages before and after SHP099 administration. Kidney function was measured, with serum blood urea nitrogen (BUN), serum creatinine, and urinary albumin-to-creatinine ratio (ACR) determined using commercial kits (Jiancheng, Nanjing, China).

Collection of Human Samples

In this study, 10 healthy volunteers, 10 patients with diabetes without nephropathy (urinary ACR <30 mg/g), and a group of patients with DN (ACR >30 mg/g) were recruited from the Second Affiliated Hospital of Zhejiang University. The basic characteristics of patients and the exclusion/inclusion criteria are shown in Supplementary Table 1. The diagnosis of diabetes complied with the criteria recommended by the World Health Organization. The determination of DN was made by two experienced nephrologists according to clinical diagnostic and image screening guidelines (18). The protocol was conducted in accordance with the Declaration of Helsinki and approved by institutional review boards at the hospital (approval no. 20210479).

Blood samples were taken from all individuals after fasting for a minimum of 8 h, and blood collection was conducted between 8:30 A.M. and 10:00 A.M., taking complete aseptic precautions. The samples were prepared for peripheral blood mononuclear cell (PBMC) extraction with a commercial kit (cat. no. P5290; Solarbio, Beijing, China). Paraffin sections were obtained for immunohistochemical staining.

Histological Analysis

Harvested kidney tissues were fixed with 4% paraformaldehyde at room temperature for 48 h and embedded in paraffin. The paraffin sections (5 μm) were stained with hematoxylin-eosin, Masson trichrome, and Sirius red, respectively, according to standard procedures. Finally, changes in renal pathology were detected with a light microscope (Leica Microsystems, Wetzlar, Germany).

For immunohistochemistry, the kidney paraffin sections from patients with diabetes/DN and mice were deparaffinized and rehydrated with graded alcohol, and antibody retrieval occurred with sodium citrate. After the blocking of serum albumin, the slides were stained with anti–phosphorylated SHP2 (p-SHP2; 1:100; cat. no. ab62322; Abcam, Cambridge, U.K.), anti–tumor necrosis factor-α (TNF-α; 1:200; cat. no. sc-52746; Santa Cruz Biotechnology, Dallas, TX), anti-F4/80 (1:300; cat. no. MCA497R; Bio-Rad Laboratories, Hercules, CA), anti-Ly6G (1:300; cat. no. ab238132; Abcam), or CD86 (1:300; cat. no. ab220188; Abcam) overnight at 4°C. After three rinses with PBS, phycoerythrin-labeled mouse anti-rabbit secondary antibody (1:500; cat. no. sc-3753; Santa Cruz Biotechnology) was incubated for 2 h at room temperature. The sections were observed under a light microscope (Leica Microsystems).

For immunofluorescence staining, the slides were incubated with primary antibodies overnight at 4°C. p-SHP2 antibody (1:300; cat. no. ab62322; Abcam), anti-CD68 (1:500; cat. no. 66231-2-Ig; Proteintech, Wuhan, China), anti-Desmin (1:300; cat. no. 5332; Cell Signaling Technology, Topsfield, MA), and anti–C-X-C motif ligand 1 (CXCL1; 1:200; cat. no. 12335-1-AP; Proteintech) were the primary antibodies used. Alternatively, secondary antibodies, including Cy3-labeled antibody (1:500; cat. no. GB21403; Servicebio, Wuhan, China) and Alexa Fluor–labeled antibody (1:500; cat. no. GB25404; Servicebio), were incubated for 2 h at room temperature in the dark. The nuclei were stained with DAPI. All stained sections were observed using a confocal microscope (A1R-SIM-STORM; Nikon, Tokyo, Japan).

Primary mouse peritoneal macrophages (MPMs) were incubated in a 24-well plate for cellular immunofluorescence staining. After treatment, cells were washed with PBS and fixed with 4% paraformaldehyde. After three rinses with PBS, cells were permeabilized with 0.1% Triton X-100. After blocking the cells with 5% BSA for 1 h, cells were cultured with primary antibodies overnight at 4°C. Anti–NF-κB p65 antibody (cat. no. 10745-1-AP; Proteintech) was used at 1:300. Cy3-conjugated donkey anti-rabbit immunoglobulin G (H+L) cross-adsorbed secondary antibody (1:300; cat. no. GB21403; Servicebio) was incubated for 2 h at room temperature in the dark. The nuclei were counterstained with DAPI. The images were observed with a confocal microscope (A1R-SIM-STORM).

Flow Cytometry

Fresh tissues were excised, minced, and digested with collagenase D (cat. no. 11088858001; Sigma-Aldrich) at 37°C for 50 min with shaking. Cell suspensions were strained through a 70-μm filter and treated with red blood cell lysis buffer (cat. no. C3702; Beyotime Biotechnology, Shanghai, China). Cells were blocked with TruStain FcX PLUS antibody (1:500; cat. no. 156603; BioLegend, San Diego, CA), and the dead cells were detected using the Zombie Aqua Fixable Viability Kit (1:100; cat. no. 423101; BioLegend). The cells were then incubated with the following conjugated antibodies for 30 min at 4°C in the dark: CD45-PE-Cy7 (1:100; cat. no. F2104505; Multisciences Biotech, Hangzhou, China), CD11b-PerCP/Cyanine5.5 (1:100; cat. no. 45-0112-80; eBioscience, San Diego, CA), F4/80-PE (1:100; cat. no. 12-4801-80; eBioscience), and Ly6G-FITC (1:200; cat. no. 127605; BioLegend). After that, the samples were washed with PBS three times, centrifuged at 400*g* for 5 min, and resuspended with 300 μL PBS. Flow cytometry was

performed using FACSCelesta instruments (BD Biosciences, San Jose, CA) and analyzed using FlowJo (version 10) software. Myeloid cells were identified as the $CD45^+/CD11b^+$ population of cells, whereas macrophages were $CD11b^+F4/80^+$ and neutrophils were $CD11b^+Ly6G^+$.

Measurement of p-SHP2 and Cytokine

The contents of p-SHP2 and pan-SHP2 were detected using a semiquantitative ELISA kit (cat. no. ab279925; Abcam) according to the manufacturer's instruction. TNF-α and interleukin-1β (IL-1β) cytokines were detected in kidney tissues or cellular supernatants using commercial ELISA kits (Anogen, Mississauga, Ontario, Canada). All readings were obtained on a microplate reader (Bio-Rad Laboratories) at 450 nm. The samples were analyzed induplicate.

Cell Isolation, Culture, and Treatments

Male $SHP2^{fl/fl}$ and SHP2-MKO mice were used for the MPM isolation assay. The mice were each intraperitoneally injected with 2 mL 6% thioglycolate solution (0.3 g beef extract, 1 g tryptone, and 0.5 g sodium chloride dissolved in 100 mL double-distilled H_2O and filtrated through a 0.22-μm filter). After 2 days, the peritoneal cells were harvested by washing the peritoneal cavity with 8 mL RPMI medium per mouse. The cells were then centrifuged at 1,000 rpm for 5 min and suspended in RPMI medium containing 11.1 mmol/L D-glucose with 10% FBS (Hyclone, Logan, UT) and 1% penicillin and streptomycin. Floating cells were removed by the medium and washed for 2 h after seeding, and adherent peritoneal macrophages were used for experiments. MPMs were maintained in a culture medium containing 21.9 mmol/L D-glucose (total 33 mmol/L; Sigma-Aldrich) and palmitic acid (PA; 100 μmol/L; Sigma-Aldrich) for 6 h to detect the mRNA levels of inflammatory cytokines.

The Shanghai Cell Bank of the Chinese Academy of Sciences (Shanghai, China) provided the RAW264.7, SV40 EM13, and NRK-52E cells. All types of cells were cultured in DMEM (Gibco, Eggenstein, Germany) supplemented with 10% FBS, 100 units/mL penicillin, and 100 units/mL streptomycin.

In cellular experiments using MPMs, SHP2 overexpression was carried out by transfecting cells with pcDNA3.1 expression HA-SHP2 plasmid (Youbio Biological Technology Co., Ltd, Changsha, China) using Lipofectamine 3000 Transfection Reagent (Invitrogen, Carlsbad, CA). After transfection for 24 h, the cells were incubated with an MAPK inhibitor mixture containing inhibitors of JNK, SP600125 (5 μmol/L), ERK, and U0126 (5 μmol/L) for 1 h.

RNA Sequencing

MPMs from $SHP2^{fl/fl}$ and SHP2-MKO mice were stimulated with high glucose (HG) and PA for 6 h and then were used for total RNA isolation with TRIzol (Invitrogen). RNA concentration was quantified by NanoDrop ND-1000 (NanoDrop, Wilmington, DE). Quality control of RNA samples was mainly conducted using an Agilent 2100 bioanalyzer (Thermo Fisher Scientific, Waltham, MA). The mRNA was purified from 1 μg total RNA using Oligo(dT)-attached magnetic beads. Then, the purified mRNA was fragmented into small pieces with fragment buffer at an appropriate temperature. Afterward, and with the use of random hexamer-primed reverse transcription, the cleaved RNA fragments were transcribed into cDNA. cDNA library construction and sequencing were performed using the BGISEQ-500 platform (Beijing Genomics Institute, Shenzhen, China). High-quality reads were aligned to the mouse reference genome using Bowtie2 (version 2.2.5) and HISAT2 (version 2.0.4). The gene expression levels were normalized to fragments per kilobase of the exon model per million mapped reads by RSEM (version 1.2.12). Differentially expressed genes (DEGs) were calculated and filtered by $P < 0.01$ and log 2 (fold change) >1.5 or <-1.5 using R package DESeq2. Gene enrichments were calculated using gene set enrichment analysis, with $P < 0.05$, false discovery rate <0.25, and normalized enrichment score >1 set as significant.

Real-Time Quantitative PCR

Total RNA was extracted from renal tissues and cells using TRIzol reagent (Invitrogen). One microgram of RNA was reversely transcribed to cDNA using Hifair III 1st Strand cDNA Synthesis SuperMix (Yeasen Biotechnology, Shanghai, China). Quantitative PCR was carried out using Hieff UNICON qPCR SYBR Green Master Mix (Yeasen Biotechnology) and the Bio-Rad CFX96 Touch Real-Time PCR Detection System (Bio-Rad Laboratories). The level of β-actin expression used allowed data normalization. The primers for *Shp2*, *Tgfb*, collagen type 4 (*Col4*), *Tnfa*, *Il1b*, *Il6*, *Il23*, *Il17*, *Cxcl1,* colony-stimulating factor 3 (*Csf3*), *Megsin*, *Myh9*, *α-SMA*, *E-cadherin*, *ZO-1*, and *Vimentin* were synthesized by Sangon Biotech (Shanghai, China) and are shown in Supplementary Table 2.

Immunoblotting

Total protein lysates of renal tissues or cells were prepared using a cell and tissue total protein extraction kit (Kang Cheng Bioengineering, Shanghai, China). The nuclear and cytoplasmic lysates were extracted using the Nuclear and Cytoplasmic Protein Extraction Kit (Beyotime Biotechnology) according to the manufacturer's instructions. Briefly, the lysates were centrifuged at 12,000 rpm and 4°C for 10 min, and the supernatant was regarded as cytoplasmic protein. The precipitation was completely suspended with nuclear protein extraction reagents and continued to decompose for 30 min at 4°C; lysates then were centrifuged at 12,000 rpm and 4°C for 10 min, and the supernatant was collected as nuclear protein. The protein concentration was measured by a BCA protein assay kit (Beyotime Biotechnology). Protein extracts were separated by SDS-PAGE and then transferred to polyvinylidene difluoride membranes. After blocking with the use of 5% nonfat milk, the membranes were incubated with antibodies against I-κB (1:1,000; cat. no. 10268-1-AP; Proteintech), NF-κB p65 (1:1,000; cat. no. 10745-1-AP;

Proteintech), SHP2 (1:1,000; cat. no. 3397; Cell Signaling Technology), p-JNK (1:2,000; cat. no. 9255; Cell Signaling Technology), JNK (1:1,000; cat. no. 9252; Cell Signaling Technology), p-ERK (1:1,000; cat. no. 28733-1-AP; Proteintech), ERK (1:1,000; cat. no. 16443-1-AP; Proteintech), Lamin B (1:1,000; cat. no. 66095-1-Ig; Proteintech), and GAPDH (1:1,000; cat. no. 60004-1-Ig; Proteintech) at 4°C overnight. After being washed with TBS-Tween buffer, the immunoreactive bands were detected by incubating them with HRP-labeled secondary antibodies. Their visualization occurred using an enhanced chemiluminescence kit (Servicebio). The band intensities were quantified using Image J software (National Institutes of Health, Bethesda, MD).

Statistical Analyses

Statistical analyses were conducted using GraphPad Prism (version 8.0.1) software (GraphPad Software, Inc., La Jolla, CA). All data are presented as mean ± SEM. A one-way ANOVA followed by Tukey post hoc test was used for multiple comparisons. An unpaired Student *t* test was selectively used for pairwise comparisons between the two groups. Statistical significance was defined as a P value <0.05, indicating the presence of a statistically significant difference.

Data and Resource Availability

Data can be obtained upon reasonable request.

RESULTS

Upregulated p-SHP2 in Macrophages of Diabetic Kidney Tissues

To investigate the potential role of SHP2 in DN, the diabetic mouse model was established by using STZ. The expression and activity of SHP2 were measured in kidney tissues, which showed that both mRNA and protein levels of SHP2 had no significant differences in the kidney tissues of T1D mice compared with those of control mice (Fig. 1*A* and *B*). However, the p-SHP2 level was significantly increased in the diabetic kidneys (Fig. 1*B* and Supplementary Fig. 1*A*). To prove the clinical importance of p-SHP2, we compared its expression in kidney tissues from patients with DN and healthy subjects, respectively. Immunohistochemical staining showed that the p-SHP2 levels in kidneys of patients with DN were much higher than in healthy kidneys (Supplementary Fig. 1*B*). SHP2 has been demonstrated to be highly expressed in macrophages (17). Therefore, immunofluorescence staining was performed to validate the primary source of the increased p-SHP2 in kidney tissues. The p-SHP2 level was evident in infiltrated $CD68^+$ macrophages other than renal mesangial cells (Desmin positive) in kidneys of diabetic mice (Fig. 1*C* and *D*). Furthermore, the results from flow cytometry showed an increased number of infiltrated $CD45^+CD11b^+F4/80^+$ macrophages and $CD45^+CD11b^+Ly6G^+$ neutrophils in kidney tissues of T1D mice (Fig. 1*E* and Supplementary Fig. 1*C* and *D*). We also showed that the level of p-SHP2 was at its peak at 1 h in the cultured MPMs challenged with HG and PA (Fig. 1*F*). These results suggest a potential role of SHP2 activity in DN.

To investigate whether increased p-SHP2 contributes to the pathogenesis of DN in humans, we detected its level in PBMCs from healthy individuals, patients with diabetes without DN, and patients with DN. Compared with those in healthy individuals, p-SHP2 levels in PBMCs gradually increased in patients with diabetes and DN, whereas SHP2 levels did not change among three groups (Fig. 1*G*). The p-SHP2 levels in these three groups were positively correlated with the ACR (Fig. 1*I*) and negatively correlated with the estimated glomerular filtration rate (Fig. 1*I*). A correlation between SHP2 and ACR or estimated glomerular filtration rate was not seen (Supplementary Figure 2). These results indicate that p-SHP2 in macrophages is involved in the progression of DN in humans.

Macrophage-Specific SHP2 Deficiency Prevented DN in T1D Mouse Model

To examine the functional role of SHP2 in DN, we generated SHP2-MKO mice, with $SHP2^{fl/fl}$ mice as littermate controls, and subjected these mice to the DN model by STZ injection (Fig. 2*A*). The efficiency of SHP2 deletion in macrophages was validated, and the MPMs from SHP2-MKO mice showed no detectable amounts of p-SHP2 or SHP2 protein (Supplementary Fig. 3). As expected, the STZ-induced diabetic mice showed increased blood glucose and decreased body-weight gains when compared with control mice, and SHP2-MKO mice showed no significant differences on these two indexes compared with $SHP2^{fl/fl}$ mice challenged with STZ (Fig. 2*B* and *C*). SHP2-MKO-T1D mice showed ameliorated renal function compared with $SHP2^{fl/fl}$-T1D mice, as evidenced by the ratio of kidney weight to body weight and the levels of BUN and creatinine (Fig. 2*D*–*F*). Furthermore, the analysis of the collected kidney tissues showed matrix expansion and glomerulosclerosis in $SHP2^{fl/fl}$-T1D mice, but not in SHP2-MKO-T1D mice (Fig. 2*G*). Masson trichrome and Sirius red staining also showed significantly increases in renal fibrosis and collagen deposition in $SHP2^{fl/fl}$-T1D mice, whereas SHP2-MKO reversed these pathological changes (Fig. 2*G*–*I*). Similarly, the transcript levels of *Col4* and *Tgfb* were remarkably elevated in kidney tissues from $SHP2^{fl/fl}$-T1D mice compared with control mice, and these diabetes-induced fibrotic changes in kidney tissues were normalized in SHP2-MKO-T1D mice (Fig. 2*J*). These findings confirm the protective role of SHP2 deficiency in macrophages against diabetes-induced renal dysfunction and pathological alterations.

SHP2 Deficiency in Macrophages Reduced Inflammation in Diabetic Mouse Kidneys

Previous studies have reported that macrophage-mediated inflammatory reaction contributes to the development of DN (19). Therefore, we determined whether SHP2 deficiency in macrophages protected kidney tissues by inhibiting infiltration and inflammatory response. Both the ELISA and real-time quantitative PCR detections of diabetic kidney

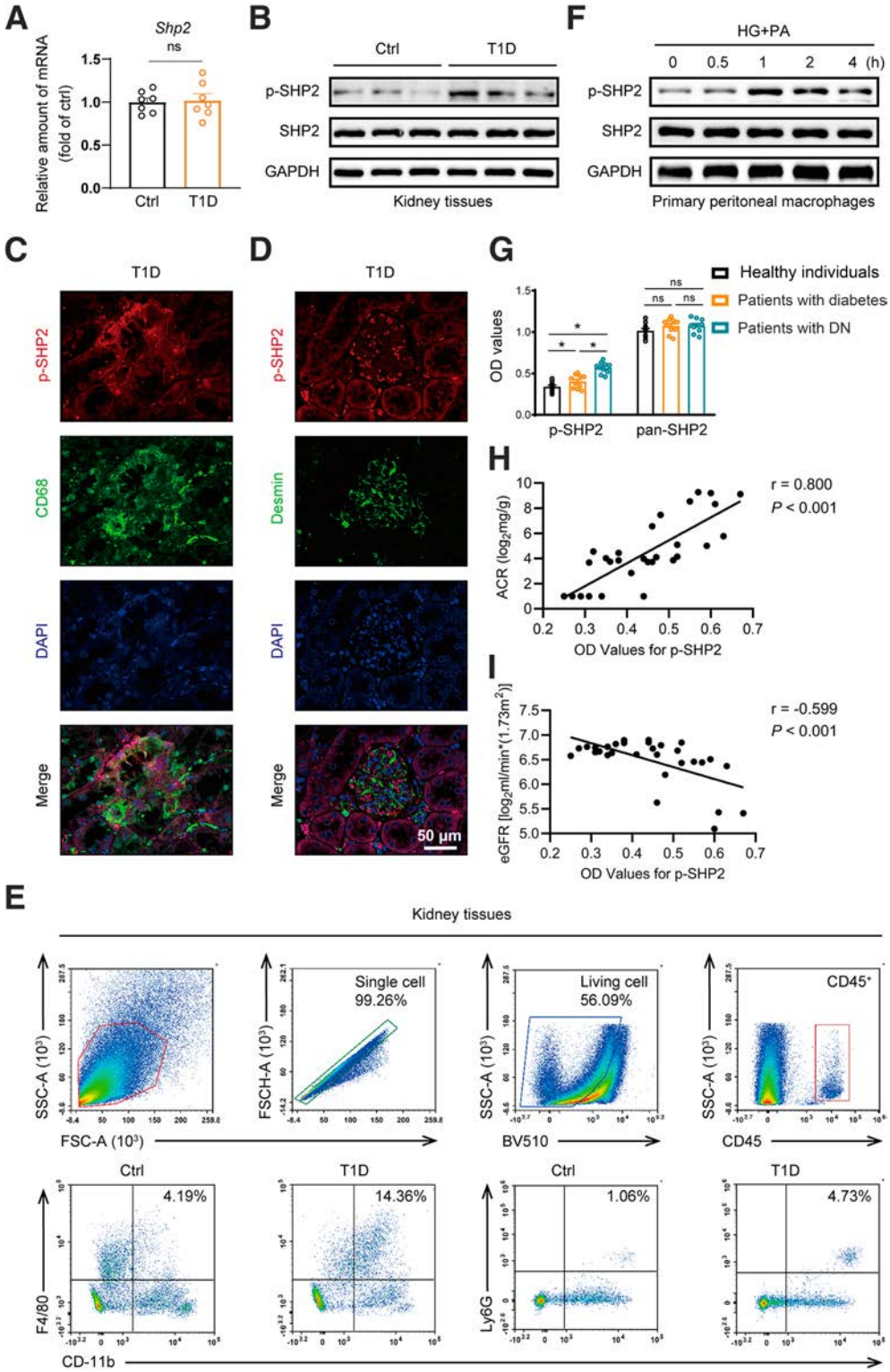

Figure 1—Role of SHP2 activation in DN pathogenesis. *A*: Relative mRNA level of *Shp2* in kidney tissues of T1D mice. *B*: Representative Western blot analysis of p-SHP2 and SHP2 levels in kidney tissues of diabetic mice. *C* and *D*: Representative immunofluorescence staining of p-SHP2 (red), CD68 or Desmin (green), and DAPI (blue) in diabetic kidney tissues. Scale bar = 50 μm. *E*: Flow cytometric analysis of percentage of $CD45^+CD11b^+F4/80^+$ macrophages and $CD45^+CD11b^+Ly6G^+$ neutrophils in the kidney. *F*: Representative Western blot analysis of p-SHP2 and SHP2 in MPMs challenged with HG+PA at different time points. *G*: Levels of p-SHP2 and pan-SHP2 in PBMCs from healthy individuals and patients with diabetes with or without DN. *H* and *I*: Correlation between optical density (OD) values of p-SHP2 in PBMCs and ACR (*H*) or estimated glomerular filtration rate (eGFR) (*I*) in patients with diabetes. Data are shown as mean ± SEM ($n = 7$ [*A*], $n = 3$, [*B–G*], and $n = 10$ [*H–J*]). *$P < 0.05$. FSC, forward scatter; ns, not significant; SSC, side scatter.

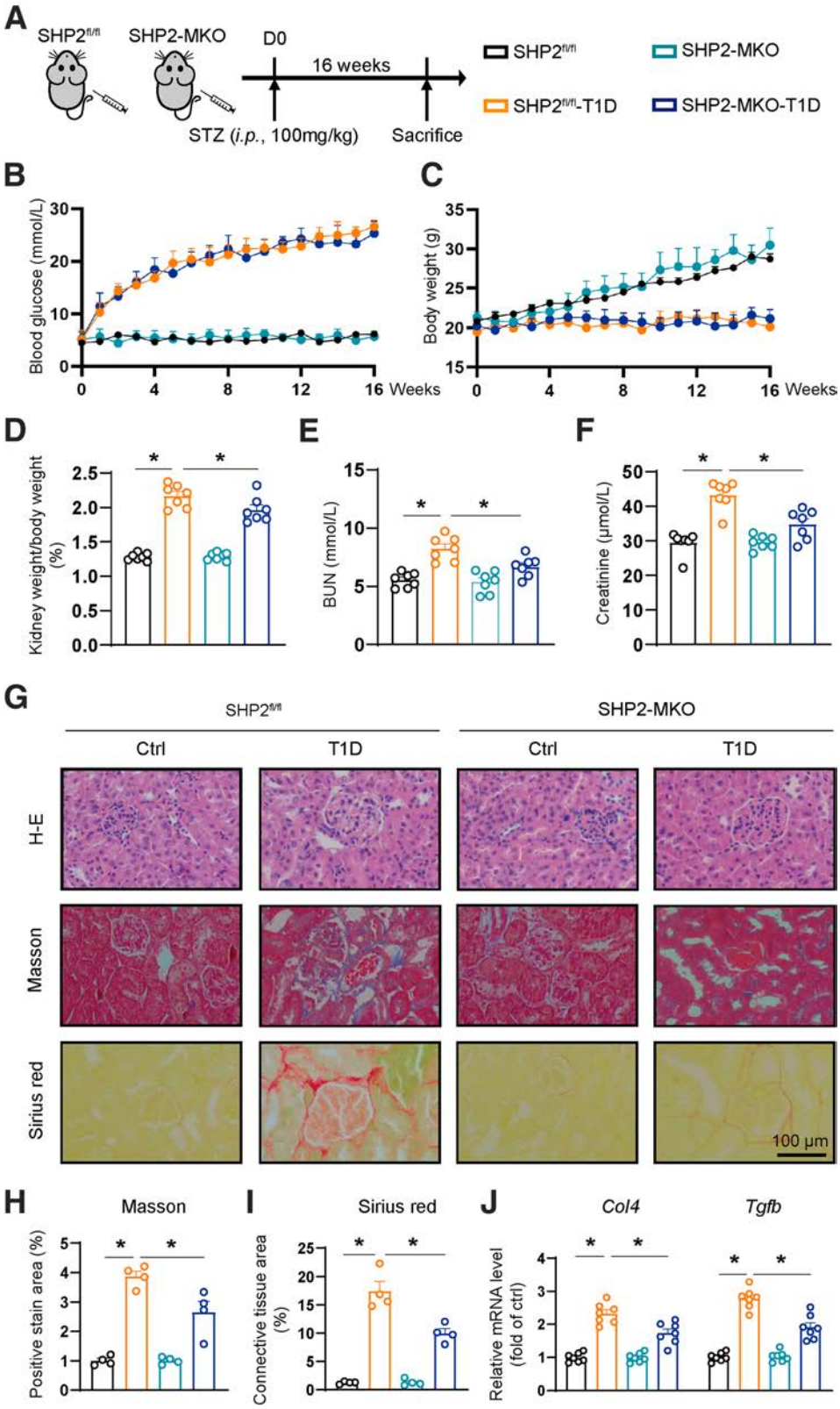

Figure 2—Macrophage-specific SHP2 deficiency attenuates renal dysfunction and fibrosis in T1D mice. *A*: SHP2-MKO mice and SHP2$^{fl/fl}$ mice at age 9 weeks were induced into T1D with STZ (100 mg/kg intraperitoneally). Age-matched SHP2-MKO and SHP2$^{fl/fl}$ mice served as control groups. After 16 weeks, mice were euthanized, and blood samples and kidney tissues were harvested. *B* and *C*: During animal experiments, blood glucose and body weight were measured every week. *D*: Percentage of kidney weight to body weight was calculated. *E* and *F*: Serum concentrations of BUN and creatinine were measured. *G*: Representative images of hematoxylin-eosin (H-E; upper), Masson trichrome (middle), and Sirius red (lower) staining of kidney tissues. Scale bar = 100 μm. *H* and *I*: Quantification of positive stain area

tissues showed that macrophage SHP2 deficiency significantly decreased the levels of TNF-α and IL-1β, as compared with the $SHP2^{fl/fl}$-T1D group (Fig. 3*A* and Supplementary Fig. 4*A* and *B*). The mRNA levels of *Il6*, *Il23*, *Cxcl1*, *Csf3*, and *Il17* were significantly elevated in $SHP2^{fl/fl}$-T1D mice, but no increases were seen in SHP2-MKO-T1D mice (Fig. 3*B* and Supplementary Fig. 4*C*). Immunohistochemical staining of TNF-α in kidney tissues was also decreased in SHP2-MKO-T1D mice compared with in $SHP2^{fl/fl}$-T1D mice (Supplementary Fig. 5*A*). This reduction of inflammatory cytokines in SHP2-MKO-T1D mice was associated with a suppression of inflammatory cell recruitment in the kidneys. The percentages of infiltrative $CD45^+CD11b^+F4/80^+$ macrophages and $CD45^+CD11b^+Ly6G^+$ neutrophils in kidney tissues of SHP2-MKO-T1D mice, as assessed by flow cytometric assay, were significantly lower than those in $SHP2^{fl/fl}$-T1D mice (Fig. 3*C*–*F*). F4/80 and Ly6G immunoreactivity assays further confirmed this result (Fig. 3*G* and Supplementary Fig. 5*B*). Notably, the $CD86^+$ M1 macrophages in the kidney tissues of SHP2-MKO-T1D mice were lower than those in $SHP2^{fl/fl}$-T1D mice (Fig. 3*G*). In parallel, immunofluorescence staining of the kidney tissues also revealed that SHP2-MKO remarkably reduced diabetes-induced macrophage infiltration and CXCL1 overexpression (Fig. 3*H*). These results indicate that the loss of SHP2 in macrophages alleviates the inflammatory response in T1D mouse kidneys.

SHP2 Deletion Ameliorated Inflammation in Macrophages by Suppressing the MAPK/NF-κB Pathway

To elucidate the molecular mechanism underlying the anti-inflammatory effect of SHP2 deficiency in macrophages, an RNA-sequencing assay was used. MPMs were isolated from $SHP2^{fl/fl}$ and SHP2-MKO mice and then treated with or without HG+PA for 6 h. The overall numbers of changed genes among these three groups are shown in Fig. 4*A* and Supplementary Fig. 6, and 1,404 DEGs were upregulated in the $SHP2^{fl/fl}$-HG+PA group but downregulated in the SHP2-MKO-HG+PA group. These DEGs were used for KEGG enrichment analysis, indicating that the MAPK and NF-κB pathways are involved in HG+PA-SHP2 signaling (Fig. 4*B* and *C*). The expression profile of MAPK/NF-κB–related inflammatory genes in macrophages also confirmed this involvement (Fig. 4*D*). Real-time quantitative PCR assay further showed that SHP2 knockout normalized HG+PA-induced gene transcription of inflammatory factors and chemokines (*Tnfa*, *Il6*, *Il1b*, *Il23*, *Cxcl1*, and *Csf3*) in both MPMs and PBMCs of mice (Fig. 4*E*–*J* and Supplementary Fig. 7*A*). Western blot assay demonstrated that MAPK components, including p-JNK and p-ERK, were significantly suppressed in the HG+PA-stimulated MPMs from SHP2-MKO mice compared with those from $SHP2^{fl/fl}$ mice (Fig. 4*K* and Supplementary Fig. 7*B* and *C*). In parallel, after HG+PA stimulation, the activation of NF-κB was significantly inhibited in SHP2-deficient MPMs, as reflected by the reduced I-κBα degradation and p65 nuclear translocation (Fig. 4*K* and *L* and Supplementary Fig. 7*D* and *E*). We also examined the levels of MAPKs and NF-κB in mouse kidney tissues, and the data showed that MAPKs and NF-κB activation were significantly suppressed in SHP2-MKO-TID mouse kidneys (Supplementary Fig. 8). Subsequently, MPMs and RAW264.7 macrophages were subjected to transfection with SHP2 plasmid to achieve an efficient overexpression of SHP2 and subsequent p-SHP2 (Supplementary Fig. 9*A*). In comparison with the control group, the overexpression of SHP2 exhibited a significant augmentation in NF-κB activation, as well as upregulated gene expression of inflammatory factors and chemokines in MPMs (Fig. 4*M* and *N* and Supplementary Fig. 9*B*). Interestingly, a mixture of MAPK inhibitors, specifically containing JNK inhibitor SP00125 and ERK inhibitor U0126, effectively attenuated the SHP2 overexpression–induced NF-κB activation and inflammatory gene expression (Fig. 4*M* and *N* and Supplementary Fig. 9*B*). Similar results were confirmed in RAW264.7 macrophages (Supplementary Fig. 10), suggesting that the MAPK signaling pathway acts as an upstream regulator of NF-κB activation. These data demonstrate the role of SHP2 in promoting inflammatory reaction through activating the MAPK/NF-κB signaling cascade.

SHP2-Driven Macrophage Inflammatory Factors Induced Renal Cell Fibrosis

Previous studies have found that the enhanced release of inflammatory cytokines in macrophages induces renal fibrosis (20). Progression of renal fibrosis also correlates with the renal tubular epithelial to mesenchymal transition and phenotypic changes in mesangial cells (21,22). We cultured MPMs from $SHP2^{fl/fl}$ mice and SHP2-MKO mice, and cells were exposed to HG+PA. The conditional medium of MPMs was then collected and applied to mesangial cells (SV40 EM13 cells) (Fig. 5*A*). After a 24-h exposure to the conditional medium from $SHP2^{fl/fl}$ MPMs challenged with HG+PA, SV40 EM13 cells showed obvious phenotypic changes, reflected by increased mRNA levels of *Megsin* and *α-SMA* and decreased *Myh9* mRNA (Fig. 5*B*). These pathological changes were accompanied by fibrotic lesions, as upregulated mRNA levels of *Col4* and *Tgfb* (Fig. 5*C*). However, the conditional medium from SHP2-MKO MPMs challenged with HG+PA failed to induce these alterations (Fig. 5*B* and *C*). Similar experiments were performed in renal tubular epithelial NRK-52E cells (Fig. 5*D*). The conditional medium from HG+PA-challenged macrophages downregulated mRNA levels of *E-cadherin* and *ZO-1*

(%) as determined by Masson trichrome staining (*H*) and connective tissue area (%) for Sirius red staining (*I*) in kidney tissues. *J*: Relative mRNA levels of *Col4* and *Tgfb* were determined with real-time quantitative PCR assay. Data are shown as mean ± SEM ($n = 7$ [*B*–*F* and *J*] and $n = 4$ [*G*–*I*]). $^*P < 0.05$.

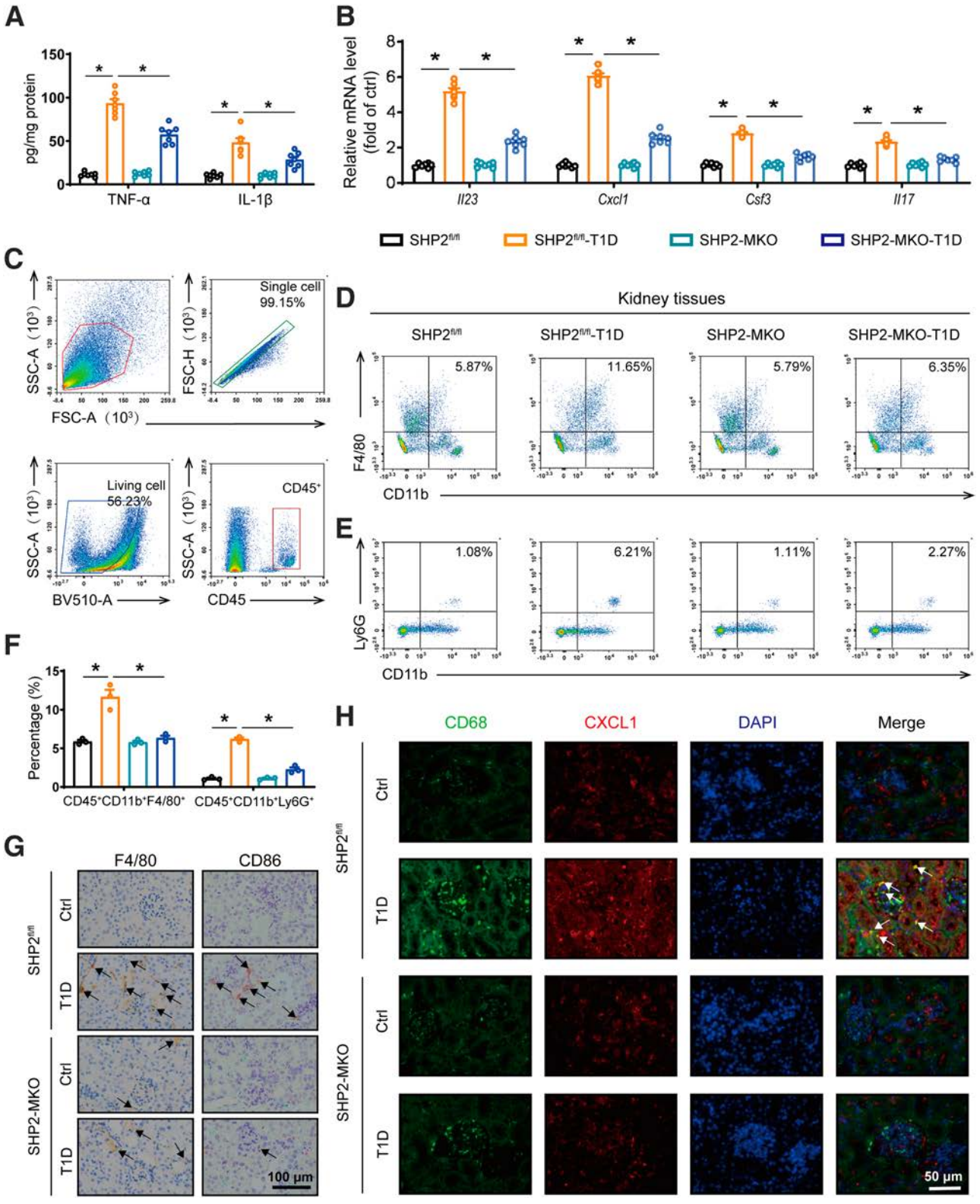

Figure 3—Macrophage-specific SHP2 deficiency improves inflammatory response in T1D mice. *A*: Concentrations of TNF-α and IL-1β in kidney tissues were detected with ELISA kits. *B*: mRNA levels of *Il23*,*Cxcl1*, *Csf3*, and *Il17* in kidney tissues. *C–F*: Flow cytometric analysis of macrophages and neutrophils in kidney tissues isolated from both SHP2-MKO mice and SHP2$^{fl/fl}$ mice challenged with STZ. *G*: Representative immunohistochemical staining of kidney tissues for F4/80 and CD86. Arrows indicate F4/80$^+$ or CD86$^+$ cells. Scale bar = 100 μm. *H*: Representative dual-immunofluorescence staining of CD68 (green) and CXCL1 (red) in murine kidney. White arrows indicate cells positive for both CD68 and CXCL1. Scale bar = 50 μm. Data are shown as mean ± SEM (n = 7 [*A* and *B*], n = 3 [*C–F*], and n = 4 [*G* and *H*]). *$P < 0.05$. FSC, forward scatter; SSC, side scatter.

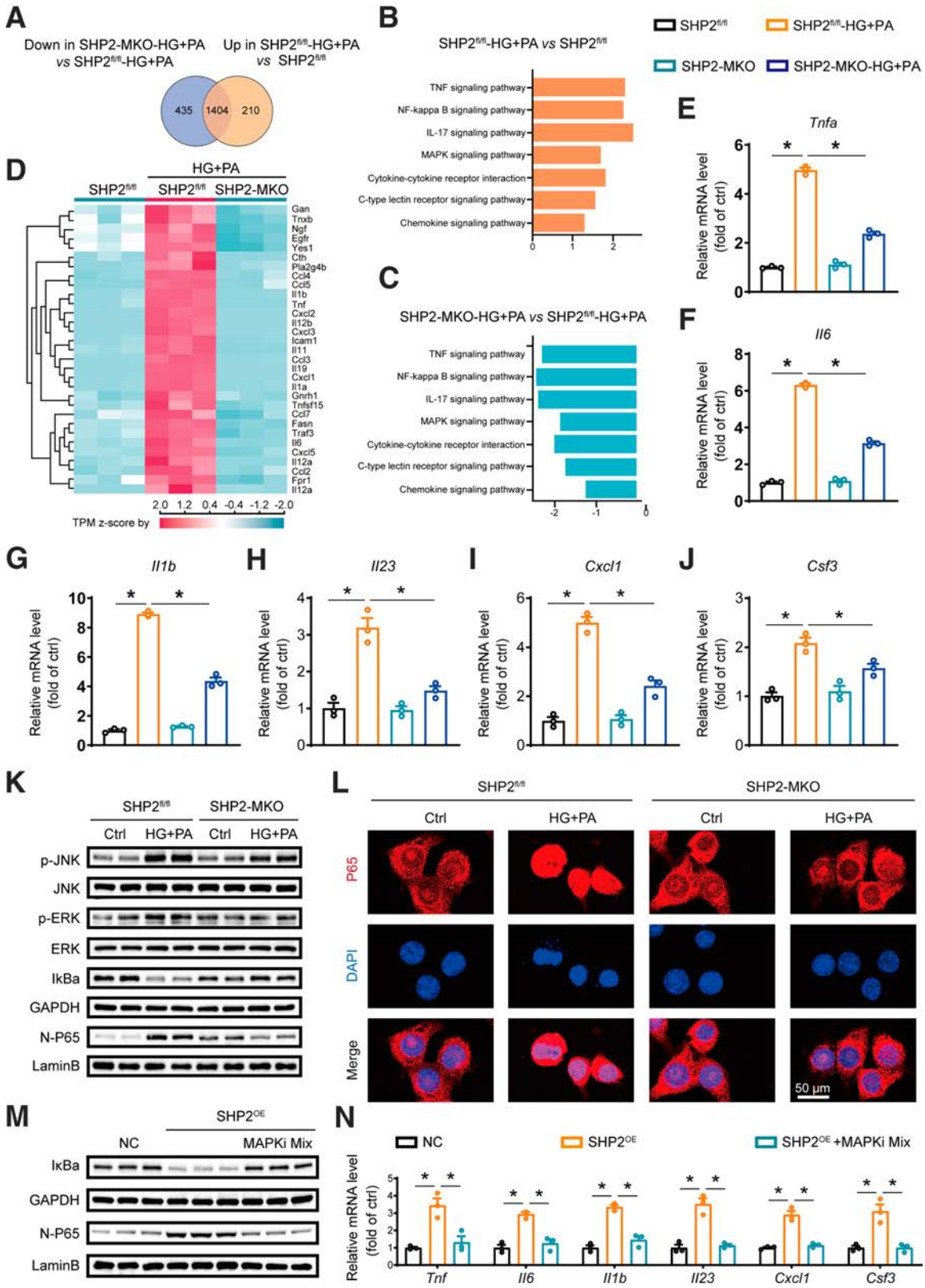

Figure 4—SHP2 deletion in macrophages inhibits inflammatory response through the MAPK/NF-κB pathway in MPMs challenged with HG and PA. MPMs from SHP2$^{fl/fl}$ mice and SHP2-MKO mice were stimulated with HG and PA for 6 h and then subjected to RNA-sequencing analysis. *A*: Venn diagram shows the number of DEGs in MPMs treated as indicated. *B* and *C*: Representative gene set enrichment analysis pathways enriched in DEGs in MPMs. *D*: Heat map of the inflammatory genes with significantly different levels in MPMs treated as indicated. *E*–*J*: Real-time quantitative PCR analysis of mRNA levels in MPMs. *K*: MPMs derived from SHP2$^{fl/fl}$ mice and SHP2-MKO mice were stimulated by HG+PA, and whole-cell lysates were used in the immunoblotting of the indicated proteins. *L*: Representative immunofluorescence

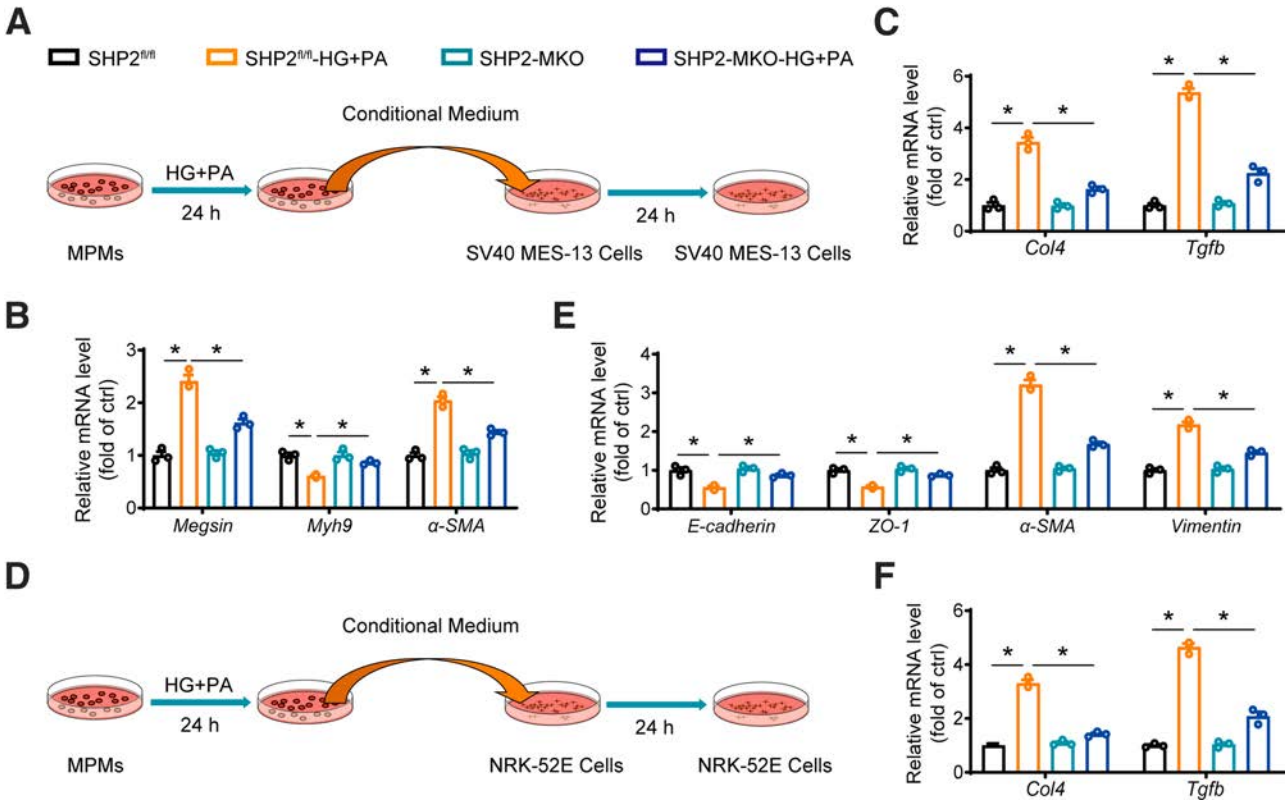

Figure 5—SHP2 is required in macrophages to induce fibrosis in renal cells. *A*: MPMs harvested from SHP2$^{fl/fl}$ mice and SHP2-MKO mice were exposed to HG+PA or vehicle for 24 h, and then the media were collected as conditional media to incubate the SV40 MES-13 cells for 24 h. *B*: Relative mRNA levels of genes related to phenotypic changes in SV40 MES-13 cells were examined by real-time quantitative PCR assay. *C*: Relative mRNA levels of fibrotic genes were measured by real-time quantitative PCR assay. *D*: Similar procedure to that in *A* was performed in NRK-52E cells. *E*: Relative mRNA levels of genes related to phenotypic changes in NRK-52E cells were examined by real-time quantitative PCR assay. *F*: Relative mRNA levels of fibrotic genes were measured by real-time quantitative PCR assay. Data are shown as mean ± SEM ($n = 3$). *$P < 0.05$.

and upregulated the *α-SMA* and *Vimentin* mRNA levels in NRK-52E cells (Fig. 5*E*), and SHP2 deficiency in MPMs prevented the cross talk between MPMs and NRK-52E cells (Fig. 5*E*). In addition, the conditional medium from SHP2-MKO macrophages could not induce *Col4* or *Tgfb* expression in NRK-52E cells (Fig. 5*F*). These data suggest that SHP2-mediated inflammatory cytokines in macrophages are responsible for phenotypic transition and fibrosis in renal mesangial cells and tubular epithelial cells, possibly through the cross talk between macrophages and renal cells.

Pharmacological Inhibition of SHP2 Attenuated DN in Mice With STZ-Induced T1D

Nine-week-old C57BL/6J mice were intraperitoneally injected with STZ to induce the T1D model. An allosteric and specific inhibitor of SHP2, namely, SHP099, was administered at doses of 2.5 and 5 mg/kg for 8 weeks in T1D mice (Fig. 6*A*). SHP099 administration did not affect changes in blood glucose or body weight in T1D mice (Fig. 6*B* and *C*). However, treatment with SHP099 resulted in a notable reduction in the percentage of kidney weight to body weight compared with the untreated T1D mice (Fig. 6*D*). Moreover, the administration of SHP099 resulted in a significant improvement in ACR, creatinine, and BUN in diabetic mice (Fig. 6*E*–*G*). Histological analysis further revealed notable improvements in renal structural abnormalities and fibrosis in the kidney tissues of SHP099-treated T1D mice compared with untreated T1D mice (Fig. 6*H*–*J*). The fibrotic alterations were also confirmed with gene markers, including *Col4* and *Tgfb* in kidney tissues (Fig. 6*K*). These findings suggest that SHP099 treatment dose-dependently benefits renal outcomes and attenuates DN in T1D mice. In addition, SHP099 administration significantly lowered *Tnfa*, *Il6*, and *Il1b* mRNA levels in T1D mouse kidneys (Fig. 6*L*). The protein levels of TNF-α and IL-1β in kidney tissues were also

staining images for p65 subunit (red) and DAPI (blue) in MPMs. Cells were stimulated with HG+PA for 1 h. Scale bar = 50 μm. MPMs were transfected with SHP2 or negative control (NC) plasmids and treated with MAPK inhibitors mixture for 1 h. *M*: Immunoblot analysis of cell lysates. *N*: Relative mRNA levels for the indicated genes. Data are shown as mean ± SEM ($n = 3$ [*A*–*J* and *L*–*N*] and $n = 4$ [*K*]). *$P < 0.05$.

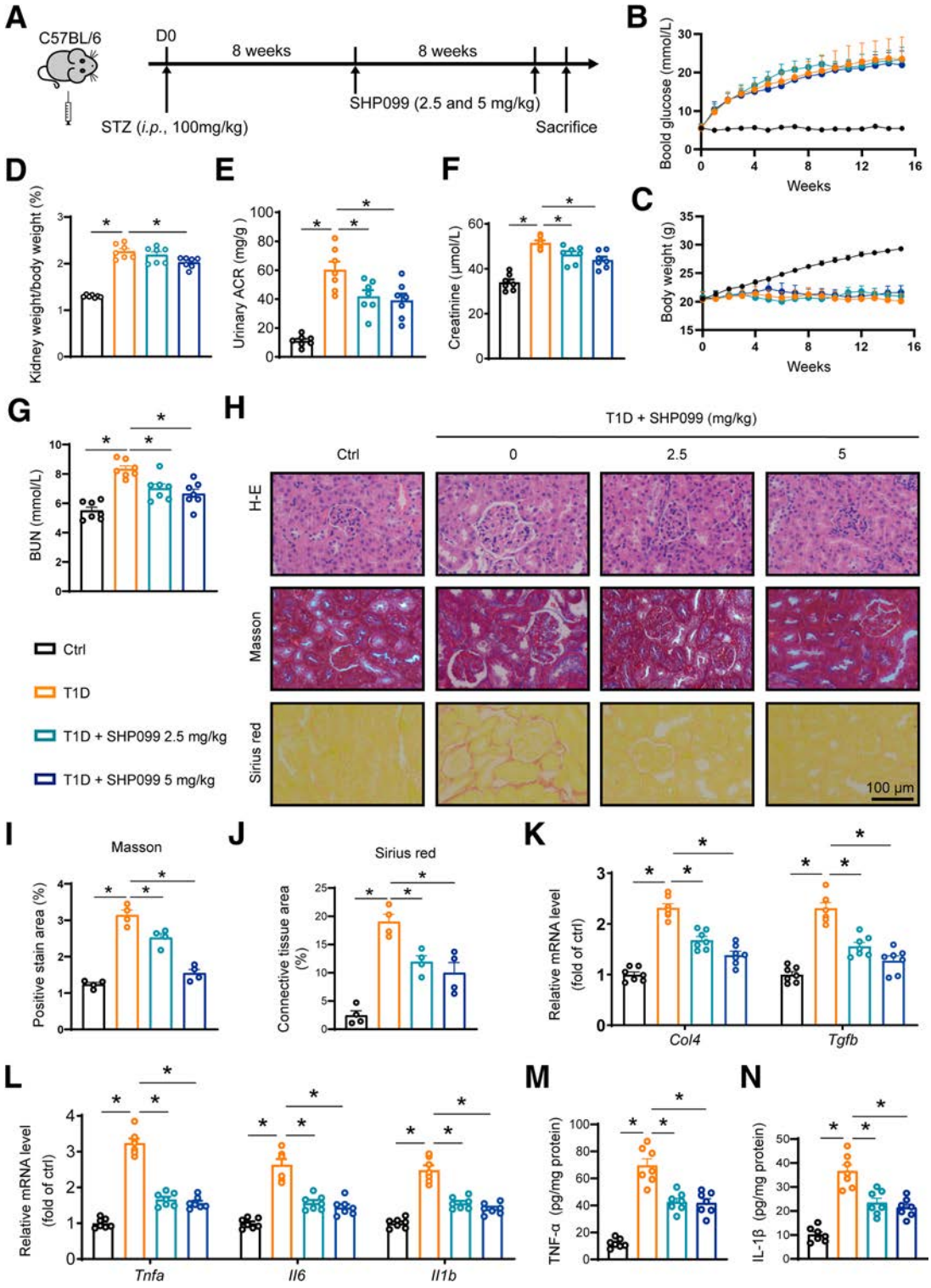

Figure 6—SHP099 treatment alleviates renal injury in STZ-induced T1D mice. *A*: Nine-week-old C57BL/6J mice intraperitoneally injected with STZ or vehicle served as the T1D mouse model or control groups. After 8 weeks, mice were treated with SHP099 (2.5 and 5 mg/kg) for the other 8 weeks, and blood samples and kidney tissues were harvested. *B* and *C*: Blood glucose (*B*) and body weight (*C*) at time points indicated. *D*: Ratio of kidney weight to body weight. *E*–*G*: Urinary level of ACR and serum levels of creatinine and BUN in T1D mice. *H*: Representative images of hematoxylin-eosin (H-E; upper), Masson trichrome (middle), and Sirius red staining (lower). Scale bar = 100 μm. *I* and *J*: SHP099 treatment significantly reduced diabetes-induced renal fibrosis. *K* and *L*: Fibrotic genes and inflammatory genes were significantly decreased by SHP099 treatment in diabetic kidney tissues. *M* and *N*: Protein levels of TNF-α and IL-1β in renal tissues were examined using ELISA kits. Data are shown as mean ± SEM ($n = 7$ [*B*–*G* and *K*–*N*] and $n = 4$ [*H*–*J*]). *$P < 0.05$.

reduced by SHP099 in a dose-dependent manner (Fig. 6*M* and *N*). As expected, SHP099 treatment of T1D mice prevented the activation of MAPK and NF-κB pathways in kidney tissues (Supplementary Fig. 11). These data suggest that pharmacological inhibition of SHP2 by SHP099 improves T1D-induced renal injury by suppressing the MAPK/NF-κB–mediated inflammatory response in vivo.

SHP2 Inhibitor Mitigated DN in the T2D Mouse Model

We conducted similar investigations using a T2D mouse model to evaluate the pharmacological effects of SHP099. The *db*/*db* mice usually begin to show symptoms of diabetes from age 8 to 10 weeks (23). The 9-week-old *db*/*db* mice were fed for total 16 weeks and administered 5 mg/kg SHP099 for the final 8 weeks, with age-matched heterozygous *db*/*m* mice as controls (Fig. 7*A*). Consistent with our results in T1D mice, SHP099 did not affect changes in blood glucose or body weight in *db*/*db* mice (Fig. 7*B* and *C*). The levels of ACR, creatinine, and BUN were increased in *db*/*db* mice, whereas these changes were reversed after SHP099 treatment (Fig. 7*D*–*F*). Assessment of renal histopathology showed that SHP099 afforded protection in structural and fibrotic changes (Fig. 7*G*). Analysis of the mRNA levels of fibrotic and inflammatory factors in kidney tissues showed significant increases in *db*/*db* mice, but not in SHP099-treated T2D mice (Fig. 7*H* and *I*). Protein levels of TNF-α and IL-1β were downregulated by SHP099 in *db*/*db* mouse kidneys (Fig. 7*J* and *K*). SHP099 treatment also inhibited the activation of MAPK and NF-κB pathways in kidney tissues of *db*/*db* mice (Supplementary Fig. 12). Thus, inhibition of SHP2 activity alleviated DN phenotypes and renal inflammation via regulating the MAPK/NF-κB signaling pathway in the T2D mouse model.

SHP099 Mitigated DN in NOD Mice

NOD mice spontaneously develop autoimmune diabetes from age 14 to 16 weeks that mimics clinical T1D (24,25). To test whether SHP2 inhibition improves autoimmune diabetes–induced renal injury, 24-week-old NOD mice were treated with SHP099 for 6 weeks (Fig. 8*A*). Blood glucose obviously increased while body weight decreased in NOD mice compared with in control NOR mice (Fig. 8*B* and *C*). SHP099 treatment did not affect blood glucose or body weight levels in NOD mice (Fig. 8*B* and *C*). The levels of ACR, creatinine, and BUN were increased in NOD mice, whereas these kidney dysfunctional markers were significantly reduced with SHP099 treatment (Fig. 8*D*–*F*). SHP099 treatment significantly attenuated renal pathology and fibrosis in NOD mice (Fig. 8*G*–*I*). Also, SHP099 treatment significantly reduced the mRNA levels of fibrotic and inflammatory factors in kidney tissues of NOD mice (Fig. 8*J* and *K* and Supplementary Fig. 13). These data confirmed that SHP099 mitigated DN in NOD mice.

In addition, we tried to examine whether the withdrawal of SHP2 inhibitor would revive DN in diabetic mice. NOD mice were treated with SHP099 for 6 weeks, and then, administration was stopped for an extra 2 weeks (Fig. 8*A*–*C*). As shown in Fig. 8*D*–*K* and Supplementary Fig. 13, SHP099-treated NOD mice with 2-week withdrawal of SHP099 showed no significant differences in any DN phenotypes or indexes when compared with the SHP099-treated group. These results indicate that the SHP099-reduced DN phenotypes would not be revived after SHP099 withdrawal.

DISCUSSION

Renal inflammation is a causative factor in hyperglycemia-induced kidney fibrosis. In the current study, we revealed that renal p-SHP2 levels were increased in both patients with DN and diabetic mice, and the p-SHP2 level was positively correlated with the progression of DN in patients. We also revealed that macrophage-specific SHP2 knockout in mouse models ameliorated diabetes-induced renal dysfunction and fibrosis, possibly associated with reduced renal inflammation. Our study elucidated the mechanisms by which SHP2 deletion mitigates DN. Specifically, SHP2 deletion suppressed the activation of MAPK and NF-κB signaling pathways, thereby inhibiting the expression of inflammatory cytokines and chemokines, including TNF-α, IL-6, IL-1β, IL-23, CXCL1, and CSF-3, as well as macrophage infiltration. These macrophage-derived cytokines promoted phenotypic transition and fibrotic responses in renal cells. Pharmacological effects of small-molecule SHP2 inhibitor against DN were examined and confirmed in both T1D and T2D mice. Collectively, our findings highlight SHP2 as a crucial regulator of DN and propose it as a promising therapeutic target for treating DN. These main findings are outlined in the graphical abstract.

In recent years, several innovative approaches aiming to provide renal protection have been proposed and investigated (26,27). However, translation of these strategies into approved therapies for treating DN remains limited. Macrophage activation responding to high levels of glucose contributes to an intricate influence between inflammation and renal parenchymal cells orchestrated by multifold cytokines/chemokines (28). A human biopsy in patients with diabetes demonstrated the emergence of macrophages in the interstitium and glomeruli at various stages of DN (29). The accumulation of macrophages in diabetic kidneys was positively associated with serum creatinine and interstitial fibrosis (30). In addition to macrophage accumulation, upregulated renal inflammatory cytokines, including TNF-α, IL-1β, and interferon-γ released from macrophages, are induced by hyperglycemia and further cause stromal hyperplasia and irreversible pathological alterations of glomeruli in kidney (31). These studies emphasize the key role of macrophage inflammation in the progression of DN. Therefore, illustrating the mechanism of macrophage inflammation and developing intervention targets in macrophages might comprise a potential treatment strategy for this disease. The C-C

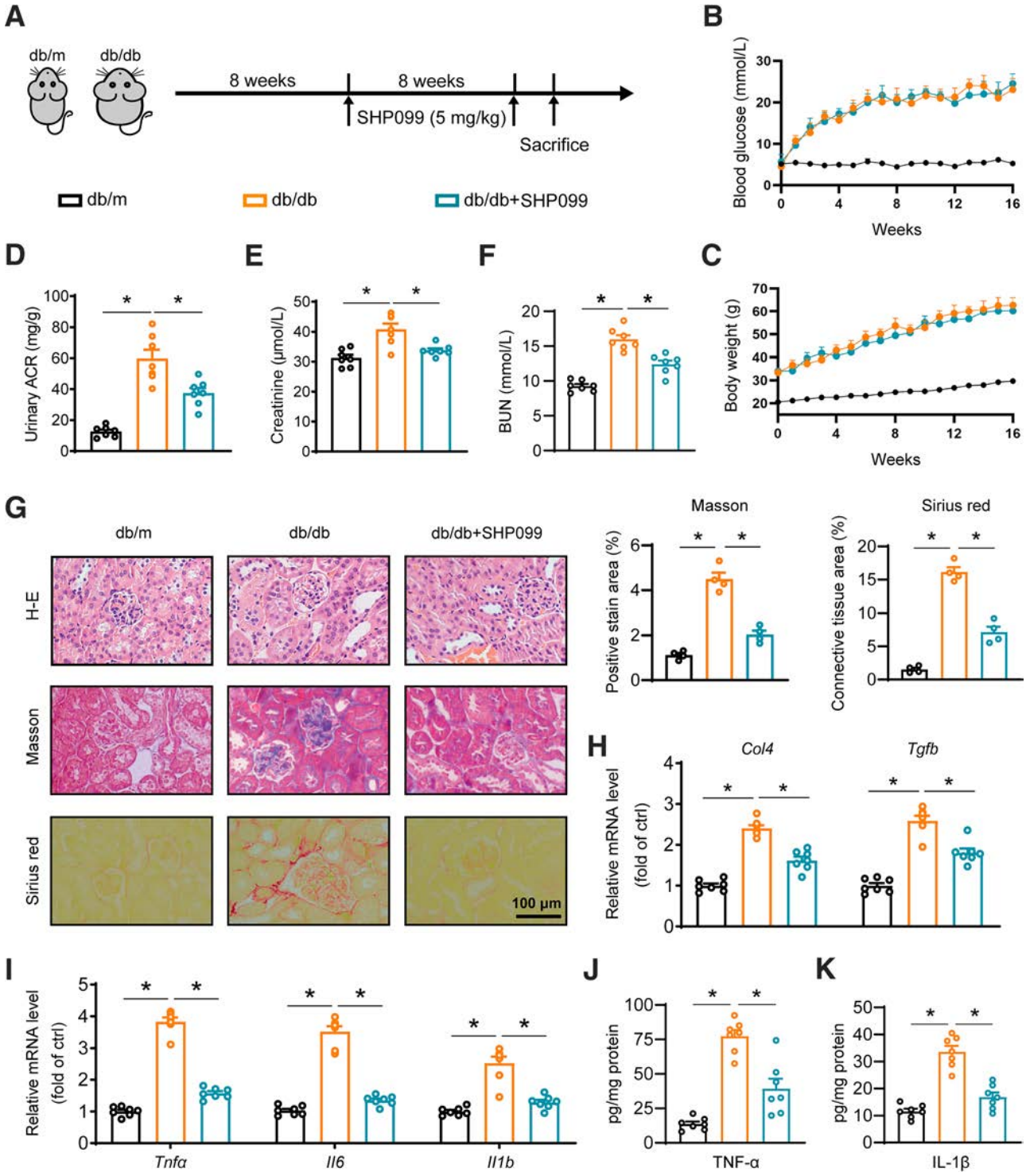

Figure 7—SHP099 suppresses renal dysfunction, fibrosis, and inflammation in *db/db* mice. *A*: For the mouse model of T2D, 9-week-old *db/db* mice were administered SHP099 (5 mg/kg) or vehicle for 8 weeks by gavage. Age-matched *db/m* mice treated with vehicle served as the control group. *B* and *C*: Blood glucose (*B*) and body weight (*C*) of mice were measured every week. *D–F*: Urinary level of ACR, serum creatinine, and BUN in *db/db* mice. *G*: Representative hematoxylin-eosin (H-E; upper), Masson trichrome (middle), and Sirius red staining (lower) images in kidney tissues, with statistical graphs on the right. Scale bar = 100 μm. *H* and *I*: mRNA levels of indicated genes. *J* and *K*: Protein levels of TNF-α and IL-1β in diabetic mouse kidneys. Data are shown as mean ± SEM ($n = 7$ [*B–F* and *H–K*] and $n = 4$ [*G*]). *$P < 0.05$.

chemokine receptor 2 antagonist CCX140-B targeting immune cells, especially macrophages, showed beneficial effects on reduction of albuminuria in patients with diabetes when administered in addition to standard treatment (30,32). Currently, phase 3 clinical trails of CCX140-B as DN treatment are planned.

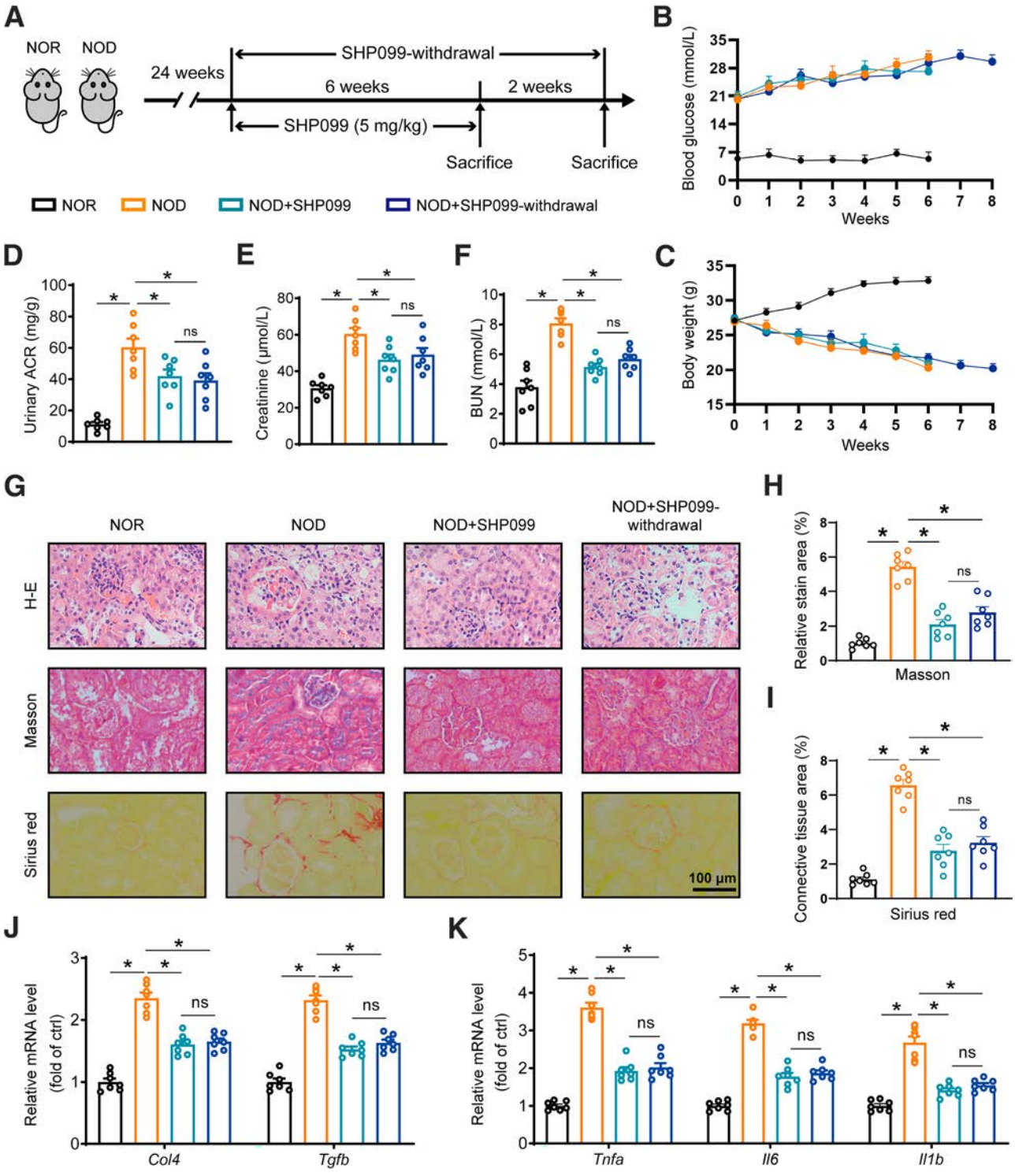

Figure 8—SHP099 treatment alleviates DN in NOD mice. *A*: Twenty-four-week-old diabetic NOD mice received SHP099 (5 mg/kg) or vehicle for 6 weeks. We also set up one group named NOD+SHP099+withdrawal, where mice were treated with SHP099 for 6 weeks (5 mg/kg) and then treated with normal saline for an extra 2 weeks. Age-matched NOR mice were treated with vehicle as the control group. *B* and *C*: Blood glucose and body weight were recorded. *D–F*: Urinary level of ACR, serum creatinine, and BUN in all mice were examined. *G*: Hematoxylin-eosin (H-E; upper), Masson trichrome (middle), and Sirius red staining (lower) were performed in kidney tissues. Scale bar = 100 μm. *H* and *I*: Relative stain areas of Masson trichrome and Sirius red were quantified. *J* and *K*: mRNA levels of indicated genes were examined by quantitative PCR assay. Data are shown as mean ± SEM ($n = 7$ [*B–F* and *J* and *K*] and $n = 4$ [*G–I*]). *$P < 0.05$. ns, not significant.

Increasing evidence has suggested that dysregulation of SHP2 disrupts critical physiological processes and various signaling pathways involved in inflammatory-mediated renal diseases (33,34). For example, knockdown of SHP2 in podocytes has been reported to prevent renal inflammation and fibrosis in mice with hyperglycemia (33). Some authors have shown that SHP2 inhibitor PHPS1 attenuates acute kidney injury via mitigating the inflammatory response mediated by the ERK-STAT3 signaling pathway (34). These studies strongly suggest a possible correlation between SHP2 and renal damage. However, the contribution of macrophage SHP2 in renal diseases is unclear so far. In this study, we found that SHP2 activation in the kidney tissues of patients with diabetes and mice and HG+PA-stimulated MPMs were much stronger than those in controls. We also showed that either diabetes or HG+PA induces SHP2 activation but not SHP2 overexpression. Because the change of macrophage SHP2 occurred only at the level of phosphorylation, instead of protein/mRNA expression, it is difficult to find the correlation between macrophage SHP2 and DN by general or single-cell RNA sequencing. This study, for the first time, shows that SHP2 activity in macrophages, rather than the expression level, is involved in diabetes-induced renal inflammation and DN. SHP099, an allosteric SHP2 inhibitor that inhibits SHP2 activation but does not influence SHP2 protein expression (16,17), was used in both T1D and T2D mice and well supported our hypothesis. We also found that the SHP099-reduced DN phenotypes were not revived after SHP099 withdrawal. Our results suggest that inhibiting the activation of SHP2 may have a direct therapeutic effect on DN, which may make the discovery of small-molecule SHP2 inhibitors as anti-DN agents favorable.

SHP2 has been investigated as a regulator of inflammation and implicated in several inflammatory-related signaling pathways through different mechanisms. We previously showed that SHP2 inhibitor suppressed excessive inflammation and increased animal survival in an acute lung injury model (16). Studies have reported that SHP2 dephosphorylates TLR7 at Tyr1024, resulting in the maintenance of the activation of the TLR7/NF-κB pathway in macrophages in the context of psoriasis (17). Mutated SHP2 associated with Noonan syndrome with multiple lentigines promoted the hyperactivation of ERK1/2 through recruiting wild-type SHP2 and subsequently enhanced MAPK activation (35). These results imply that SHP2-mediated MAPK and NF-κB signaling is critical for regulating inflammation in macrophages. Our results from RNA sequencing revealed the profile of cytokines/chemokines modulated by SHP2 deletion in macrophages, pointing out the implication of MAPK and NF-κB pathways. Our in vivo and in vitro experiments further verified the regulation of SHP2 on MAPK/NF-κB. Notably, the MAPK inhibitor mixture hampered the SHP2 overexpression–induced activation of NF-κB. These results indicate SHP2 is a positive regulator of the inflammatory response via the MAPKs/NF-κB pathway in the context of diabetes.

Renal fibrosis is characterized by fibrotic tissue replacement of functional parenchyma within the various cell types, especially the renal tubular epithelial cells and glomerular mesangial cells (22,36). Epithelial to mesenchymal transition is the process of epithelial cells transforming into interstitial cells and has been regarded as the main mechanism of interstitial myofibroblast production in renal fibrosis (21). After injury, renal epithelial cells secrete various profibrotic cytokines, such as TGF-β and Col-4, aggravating renal fibrosis (37). Furthermore, the glomerulus mesangial cells also display the accumulation of fibrogenic genes, including *Tgfb* and *Col4*, in response to HG stimulation (38). The cross talk between renal cells and macrophages plays crucial roles in the pathogenesis of DN. The inflammatory cytokines secreted by the infiltrated macrophages significantly induce the phenotypic transition and fibrosis in renal cells (39). In the current study, we found that macrophage-derived cytokines in medium resulted in the phenotypic transition of NRK-52E and SV40 EM13 cells. At the same time, these effects were not seen in SHP2 deletion in macrophages, implying that SHP2-drived macrophage cytokines induce phenotypic transition and fibrosis of the kidney. Given that macrophage inflammation is also closely implicated in other diabetic complications, such as diabetic cardiomyopathy (40,41), the therapy of SHP2 inhibition may also be effective in the treatment of other complications. This is worth exploring in the future.

In conclusion, our study provides compelling evidence that hyperglycemia triggers the activation of SHP2 and activates the SHP2-MAPK/NF-κB proinflammatory signaling pathway in macrophages, leading to renal fibrosis and dysfunction. Notably, macrophage deficiency of SHP2 and pharmacological inhibition of SHP2 each effectively attenuates the renal inflammatory response and prevents the progression of DN. Our findings therefore highlight the therapeutic potential of targeting SHP2 for DN, offering a promising avenue for therapy for inflammatory diabetic complications.

Funding. This study was supported by Zhejiang Provincial Key Scientific Project grant 2021C03041 (G.L.), Zhejiang Provincial Medicine and Health Science and Technology Project grant 2024KY932 (X.H.), and Natural Science Foundation of Zhejiang Province grant LTGD24C040007 (Q.S.).

Duality of Interest. No potential conflicts of interest relevant to this article were reported.

Author Contributions. X.H. and J.W. performed the in vitro studies and wrote the manuscript. R.Z., Y.T., M.W., L.C., and Z.X. conducted the animal work. L.Z. and C.Z. performed the imaging work. Q.S., H.Y., and G.L. conceived the project and designed the study. X.H. is the guarantor of this work and, as such, had full access to all the data in the study and takes responsibility for the integrity of the data and the accuracy of the data analysis.

References

1. Hu Q, Chen Y, Deng X, et al. Diabetic nephropathy: focusing on pathological signals, clinical treatment, and dietary regulation. Biomed Pharmacother 2023;159:114252

2. Du L, Chen Y, Shi J, et al. Inhibition of S100A8/A9 ameliorates renal interstitial fibrosis in diabetic nephropathy. Metabolism 2023;144:155376

3. Wang Z, Wu Q, Wang H, et al. Diosgenin protects against podocyte injury in early phase of diabetic nephropathy through regulating SIRT6. Phytomedicine 2022;104:154276
4. Chen J, Liu Q, He J, Li Y. Immune responses in diabetic nephropathy: pathogenic mechanisms and therapeutic target. Front Immunol 2022;13:958790
5. Cui X, Li Y, Yuan S, et al. Alpha-kinase1 promotes tubular injury and interstitial inflammation in diabetic nephropathy by canonical pyroptosis pathway. Biol Res 2023;56:5
6. Li HD, You YK, Shao BY, et al. Roles and crosstalks of macrophages in diabetic nephropathy. Front Immunol 2022;13:1015142
7. Sahakyan G, Vejux A, Sahakyan N. The role of oxidative stress-mediated inflammation in the development of T2DM-induced diabetic nephropathy: possible preventive action of tannins and other oligomeric polyphenols. Molecules 2022;27:9035
8. Awad AS, You H, Gao T, et al. Macrophage-derived tumor necrosis factor-α mediates diabetic renal injury. Kidney Int 2015;88:722–733
9. Brosius FC 3rd. New insights into the mechanisms of fibrosis and sclerosis in diabetic nephropathy. Rev Endocr Metab Disord 2008;9:245–254
10. Usui HK, Shikata K, Sasaki M, et al. Macrophage scavenger receptor-a-deficient mice are resistant against diabetic nephropathy through amelioration of microinflammation [published correction appears in Diabetes 2007;56:897]. Diabetes 2007;56:363–372
11. Dorenkamp M, Nasiry M, Semo D, et al. Pharmacological targeting of the RAGE-NFκB signalling axis impedes monocyte activation under diabetic conditions through the repression of SHP-2 tyrosine phosphatase function. Cells 2023;12:513
12. Kim C, Baek SH, Um JY, Shim BS, Ahn KS. Resveratrol attenuates constitutive STAT3 and STAT5 activation through induction of PTPε and SHP-2 tyrosine phosphatases and potentiates sorafenib-induced apoptosis in renal cell carcinoma. BMC Nephrol 2016;17:19
13. Dong B, Gao Y, Zheng X, et al. T cell activation is reduced by the catalytically inactive form of protein tyrosine phosphatase SHP-2. Int J Clin Exp Med 2015;8:6568–6577
14. Zhang Y, Cai B, Li Y, et al. Identification of linderalactone as a natural inhibitor of SHP2 to ameliorate CCl_4-induced liver fibrosis. Front Pharmacol 2023;14:1098463
15. Asmamaw MD, Shi XJ, Zhang LR, Liu HM. A comprehensive review of SHP2 and its role in cancer. Cell Oncol (Dordr) 2022;45:729–753
16. Ye S, Zuo B, Xu L, et al. Inhibition of SHP2 by the small molecule drug SHP099 prevents lipopolysaccharide-induced acute lung injury in mice. Inflammation 2023;46:975–986
17. Zhu Y, Wu Z, Yan W, et al. Allosteric inhibition of SHP2 uncovers aberrant TLR7 trafficking in aggravating psoriasis. EMBO Mol Med 2022;14:e14455
18. Zhang H, Zuo JJ, Dong SS, et al. Identification of potential serum metabolic biomarkers of diabetic kidney disease: a widely targeted metabolomics study. J Diabetes Res 2020;2020:3049098
19. Jiang WJ, Xu CT, Du CL, et al. Tubular epithelial cell-to-macrophage communication forms a negative feedback loop via extracellular vesicle transfer to promote renal inflammation and apoptosis in diabetic nephropathy. Theranostics 2022;12:324–339
20. Gondaliya P, P Dasare A, Jash K, Tekade RK, Srivastava A, Kalia K. miR-29b attenuates histone deacetylase-4 mediated podocyte dysfunction and renal fibrosis in diabetic nephropathy. J Diabetes Metab Disord 2019;19:13–27
21. Zhang HF, Liu HM, Xiang JY, et al. Alpha lipoamide inhibits diabetic kidney fibrosis via improving mitochondrial function and regulating RXRα expression and activation. Acta Pharmacol Sin 2023;44:1051–1065
22. Zhang J-L, Du C, Poon CC-W, et al. Structural characterization and protective effect against renal fibrosis of polysaccharide from *Ligustrum lucidum* Ait. J Ethnopharmacol 2023;302:115898
23. Sharma K, McCue P, Dunn SR. Diabetic kidney disease in the *db*/*db* mouse. Am J Physiol Renal Physiol 2003;284:F1138–F1144
24. Roca-Ho H, Palau V, Gimeno J, Pascual J, Soler MJ, Riera M. Angiotensin-converting enzyme 2 influences pancreatic and renal function in diabetic mice. Lab Invest 2020;100:1169–1183
25. Tochino Y. The NOD mouse as a model of type I diabetes. Crit Rev Immunol 1987; 8:49–81
26. Hu S, Wang J, Liu E, et al. Protective effect of berberine in diabetic nephropathy: a systematic review and meta-analysis revealing the mechanism of action. Pharmacol Res 2022;185:106481
27. Anders HJ, Peired AJ, Romagnani P. SGLT2 inhibition requires reconsideration of fundamental paradigms in chronic kidney disease, 'diabetic nephropathy', IgA nephropathy and podocytopathies with FSGS lesions. Nephrol Dial Transplant 2022;37:1609–1615
28. Gok MG, Paydas S, Boral B, Onan E, Kaya B. Evaluation of eryptosis in patients with chronic kidney disease. Int Urol Nephrol 2022;54:2919–2928
29. Klessens CQF, Zandbergen M, Wolterbeek R, et al. Macrophages in diabetic nephropathy in patients with type 2 diabetes. Nephrol Dial Transplant 2017;32:1322–1329
30. Calle P, Hotter G. Macrophage phenotype and fibrosis in diabetic nephropathy. Int J Mol Sci 2020;21:2806
31. You H, Gao T, Cooper TK, Brian Reeves W, Awad AS. Macrophages directly mediate diabetic renal injury. Am J Physiol Renal Physiol 2013;305: F1719–F1727
32. Minton K. Macrophages: a transcription factor to call their own. Nat Rev Immunol 2011;11:74
33. Hsu MF, Ito Y, Afkarian M, Haj FG. Deficiency of the Src homology phosphatase 2 in podocytes is associated with renoprotective effects in mice under hyperglycemia. Cell Mol Life Sci 2022;79:516
34. Jiang J, Hu B, Chung CS, et al. SHP2 inhibitor PHPS1 ameliorates acute kidney injury by Erk1/2-STAT3 signaling in a combined murine hemorrhage followed by septic challenge model. Mol Med 2020;26:89
35. Zhu G, Xie J, Kong W, et al. Phase separation of disease-associated SHP2 mutants underlies MAPK hyperactivation. Cell 2020;183:490–502.e18
36. Li H, Dixon EE, Wu H, Humphreys BD. Comprehensive single-cell transcriptional profiling defines shared and unique epithelial injury responses during kidney fibrosis. Cell Metab 2022;34:1977–1998.e9
37. Zheng C, Huang L, Luo W, et al. Inhibition of STAT3 in tubular epithelial cells prevents kidney fibrosis and nephropathy in STZ-induced diabetic mice. Cell Death Dis 2019;10:848
38. Yang X, Luo W, Li L, et al. CDK9 inhibition improves diabetic nephropathy by reducing inflammation in the kidneys. Toxicol Appl Pharmacol 2021;416: 115465
39. Zhou X, Chen H, Hu Y, et al. Enhancer of zeste homolog 2 promotes renal fibrosis after acute kidney injury by inducing epithelial-mesenchymal transition and activation of M2 macrophage polarization. Cell Death Dis 2023;14:253
40. Widiapradja A, Kasparian AO, McCaffrey SL, et al. Replacement of lost substance P reduces fibrosis in the diabetic heart by preventing adverse fibroblast and macrophage phenotype changes. Cells 2021;10:2659
41. Jia C, Chen H, Wei M, et al. Gold nanoparticle-based miR155 antagonist macrophage delivery restores the cardiac function in ovariectomized diabetic mouse model. Int J Nanomedicine 2017;12:4963–4979